J. Fluid Mech. (1988), *vol.* 191, *pp.* 535–556
Printed in Great Britain

An experimental study of homogeneous lenses in a stratified rotating fluid

By KATHERINE HEDSTROM† AND LAURENCE ARMI
Scripps Institution of Oceanography, University of California at San Diego,
La Jolla, CA 92093, USA

(Received 16 February 1987 and in revised form 4 September 1987)

Injection of a homogeneous fluid into a linearly stratified and rotating background fluid produced anticyclonic lenses which were studied for up to 600 rotation periods. Velocity measurements showed that the interior core rotates as a solid body with a decreasing, nearly axisymmetric exterior velocity field. Gill's (1981) model predicts well both the velocity and aspect ratio *vs.* Rossby number of the lenses. Lens decay occurred in two stages: symmetric rapid spin-down, with an associated half-life of ≈ 70 rotation periods followed by asymmetric shedding at a nearly constant core Rossby number, $Ro \approx 0.06$.

1. Introduction

Isolated compact anticyclonic eddies or lenses have recently been observed in a variety of oceanic locations. Armi & Zenk (1984) found three such lenses in the Canary Basin. These lenses were centred at a depth of ≈ 1100 m with a vertical extent of up to 900 m and radii of ≈ 50 km. Anticyclonic velocities as high as 29 cm s^{-1} and salinity anomalies of 0.8% were recorded. Other examples include Arctic Ocean eddies (Manley & Hunkins 1985) and compact eddies in the Sargasso Sea (Dugan *et al.* 1982). Thicknesses at lens centre as small as 25 m have been observed; small lenses are nearly homogeneous while large ones have more complicated density distributions. McWilliams (1985) reviewed both observations and theories for this class of eddy, naming them submesoscale coherent vortices. They are often long lived, with total lifetimes extending up to several years.

Previous experimental work has been primarily for two-layer systems. Saunders (1973) created a baroclinic vortex by removing a thin-walled cylinder containing fluid of a higher density from within a rotating fluid with finite depth. The stability of the vortices associated with the collapse of the cylinder of fluid was examined. Griffiths & Linden (1981) released a column of buoyant fluid at a free surface or used a continuous source of buoyant fluid at the free surface to generate an eddy which was unstable to azimuthal disturbances. Griffiths & Linden also discuss three experiments with a continuous point source in a linearly stratified fluid. In these experiments the lenses always became unstable. Griffiths & Linden claim that this occurred when the available energy of the volume of fluid injected was sufficient to amplify non-axisymmetric disturbances.

In the experiments reported here, careful injection through a diffuser produced stable lenses of various volumes. Our experiments also differed fundamentally from the trial experiments reported by Griffiths & Linden in that once a desired lens volume was achieved, the injection was stopped. The resultant lenses were studied

† Present address: Institute for Naval Oceanography, NSTL, MS 39529, USA.

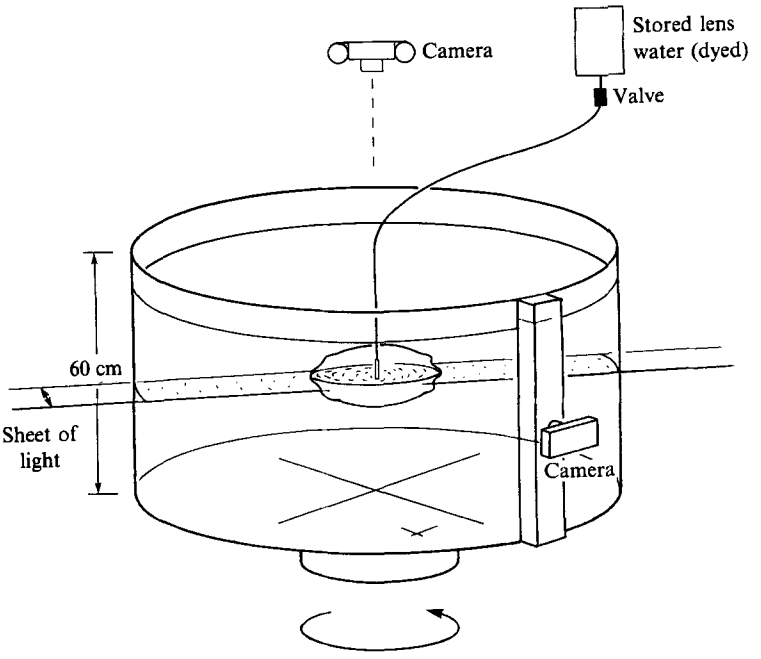

FIGURE 1. Schematic drawing of the rotating tank.

for up to 600 table rotations (approximately two hours). Flow visualization using a dyed injection and streak photographs at various levels enabled us to document details of lens decay. Velocities determined from the streak photographs show clearly the evolution of the velocity field along with changes of derived quantities such as lens core Rossby number. Early results of these experiments were reported by Hedstrom (1985, 1986).

Throughout the paper we shall make extensive use of Gill's (1981) model, comparing it with our data. Gill's model is the only lens model that includes the velocity field in the stratified fluid exterior to the injected homogeneous fluid. This is in contrast to simplified models such as Dugan *et al.*'s (1982) which ignore the exterior motion, yielding unrealistic aspect ratios *vs.* Rossby number, as well as failing to predict the exterior motion.

2. Experimental facility

Ideally, a lens is formed in fluid that is linearly stratified and rotating as a solid body. As shown in figure 1 an acrylic cylindrical tank 60 cm deep and 120 cm in diameter was permanently mounted on a rotating table. Rotation periods T ranged from 4.7 s to 22.7 s corresponding to $f = 2\Omega$ from 0.55 to 2.7 s^{-1}. The rotating table was designed with precision journal bearings under hydraulic pressure to minimize vibration and wobble. The important parameters for the experiments discussed in this paper are presented in table 1.

The tank was filled as it was rotating using the double bucket technique to produce a linear salt stratification with a free surface. Densities were measured with a hydrometer and corresponded to a range of the buoyancy frequency N from 0.48 to 1.2 s^{-1}. After filling, residual motions were allowed to decay to near solid-body rotation. Figure 2 is an example of the residual flow before a lens was injected; the

N/f	Symbol	N (s)$^{-1}$	f (s)$^{-1}$	Q (ml s^{-1})	V (l)	In figure(s)
0.18	—	0.48	2.63	Not measured		4
0.21	—	0.37	1.79	8	1.4	18
0.22	▲	0.40	1.88	8	1.0	2, 11, 12
0.36	+	0.65	1.80	8	1.1	11, 12, 14
0.48	—	0.91	1.87	7	1.1	16
0.53	—	0.72	1.35	Not measured	6, 7	
0.58	■	1.03	1.78	7	1.3	11, 12
0.80	●	1.01	1.27	6	1.1	8, 10, 11, 12, 17, 18
1.04	○	1.16	1.11	5	1.9	11, 12, 18
1.16	△	1.09	0.94	7	1.2	11, 12
1.19	□	1.19	1.00	6	1.9	3, 9, 11, 12, 13, 15
1.25	—	0.84	0.67	Not measured		5

TABLE 1. Important parameters for the experiments

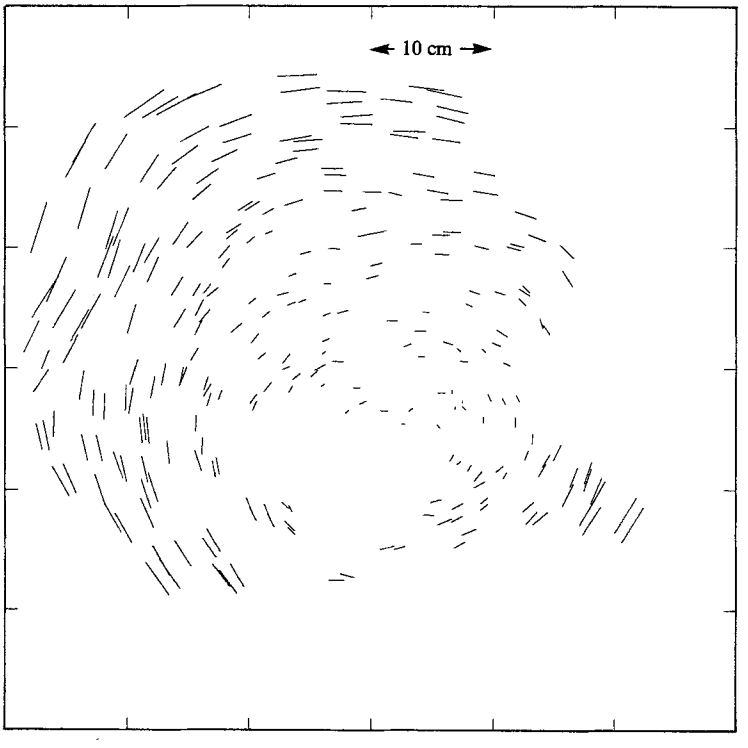

FIGURE 2. Residual motion in the tank before lens injection. $Ro = 3 \times 10^{-1}$.

length of the lines indicates the distance travelled by particles in 20 s. The Rossby number of this flow is only 3×10^{-3}.

Water injected to generate the lens was diffused through an aquarium air-stone at the depth of equivalent density. The details of the injection are important to the initial potential vorticity of the lens (see §4).

The flows were photographed from above and from the side, with distortion of the side view being removed with a small flat-surfaced container of water attached to the curved tank wall. The cameras were triggered automatically by an interval-

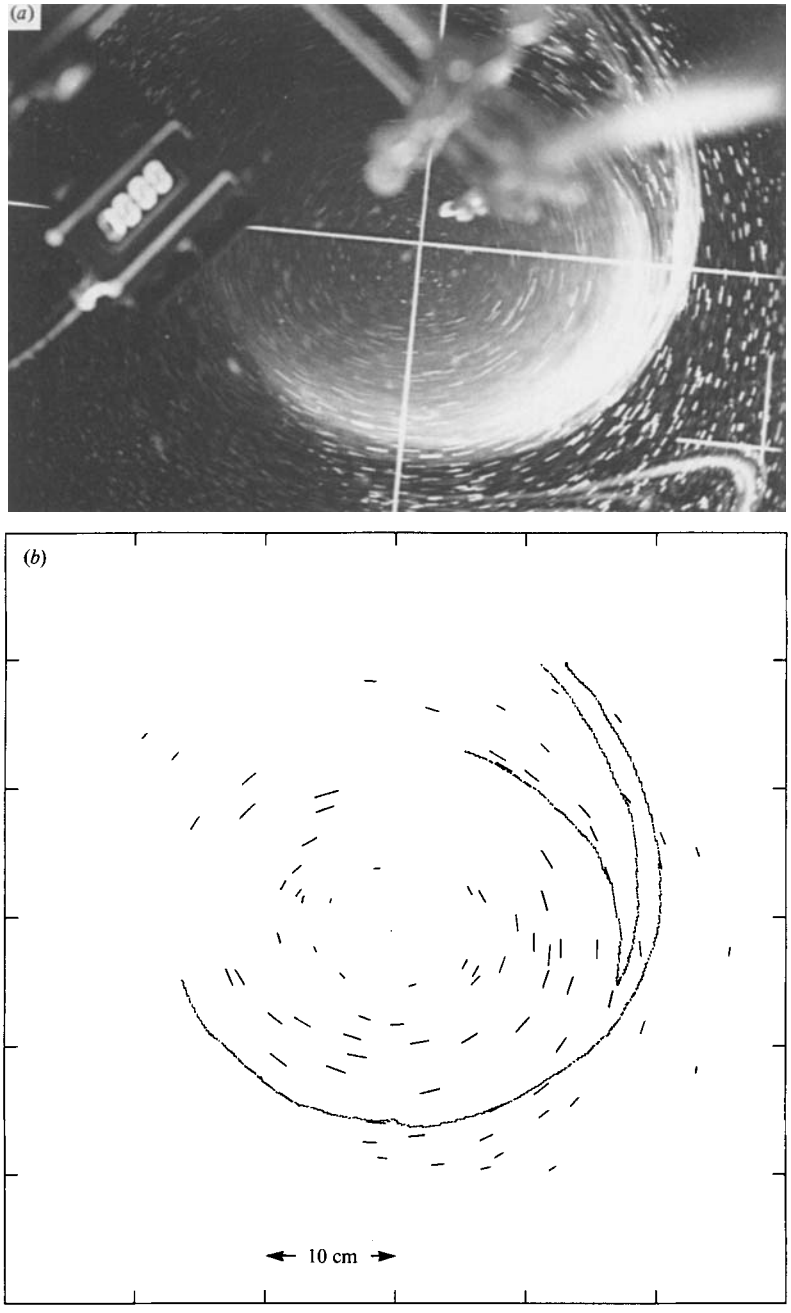

FIGURE 3. (*a*) Photograph from above a lens. $N/f = 1.19$, $t = 300$ s ($24T$ after injection, the clock in the photo shows time in min and s since the injection started). (*b*) Corrected, digitized image of streaks from (*a*).

ometer at intervals which changed from experiment to experiment and were typically 10–30 s. The interval between pictures was further adjusted so as to achieve identical lighting conditions for all of the photographs; the cameras were triggered at only one position during a rotation.

The lens water was dyed with fluorescein to distinguish it from the exterior fluid. The particles used for streak photography were pliolite with diameters of 0.3–0.4 mm and mean density 1.026. These particles were injected into the fluid just after the tank was filled and became well distributed in the horizontal. During a slightly turbulent lens injection some of the particles were entrained into the lens; laminar injections entrained insufficient particles and in these cases it was necessary to inject additional particles directly into the lens using a device similar to that used to produce the lens itself.

Particle-streak photography requires a long exposure time for adequate velocity determination. A camera with an electronically timed and calibrated shutter was used with an exposure time of 1.020 ± 0.005 s. The depth of particle streaks appearing in photographs was controlled by illuminating the tank with a horizontal sheet of light. This was produced with a slit mask made from a projector slide, the level of the projected light sheet being determined by the location of the slit. A sequence of such slides was arranged in a projector carousel. The velocity field was obtained from the length of particle streaks on slides projected onto a digitizing tablet. Perspective was accounted for numerically, using the height of illuminated particles above a scale on the tank floor. The surface curvature of the fluid results in only a small additional correction, which was ignored. Figure 3(*a*) is an example of a streak photograph; its corrected digitized image is shown in figure 3(*b*) where the outline of the dyed lens water has also been included. The velocity fields were derived from these corrected digitized images.

3. Aspect ratios and axisymmetric instabilities

This section contains a description of lens shapes observed with diffuse illumination. Gill's (1981) model predicts that the aspect ratio at any Rossby number is proportional to f/N. The effect of f/N is shown in the photographs of three different lenses in figures 4, 5, and 6(*a*). These photographs were taken early in each experiment, during the laminar injection, so as to minimize effects of mixing and diffusion. This laminar injection technique ideally produces a lens with zero potential vorticity, corresponding to a Rossby number of 0.5, which is approximated by our observations discussed in §4. Throughout the paper, we shall define the Rossby number as $Ro = \omega/f$, where ω is the angular frequency of the lens core (half the core vorticity). The experiments were carried out with values of f/N varying by a factor of 5; the aspect ratio α varied by a corresponding amount.

With viscous decay, lens aspect ratios decrease, corresponding to smaller pressure gradients needed to balance reduced Coriolis forces. Figure 7 shows the aspect ratio as a function of time for the lens shown in figure 6(*a*). The aspect ratio is an ambiguous measurement compared to the Rossby number; its measurement is also complicated for non-axisymmetric lenses as described in §6, as well as for lenses which develop axisymmetric instabilities.

Figure 6(*a–c*) shows one lens at three successive times as seen from the side. It is evident that an axisymmetric instability has appeared. The growth rate for this instability is on the order of 10–30 revolutions, with a vertical spatial scale of

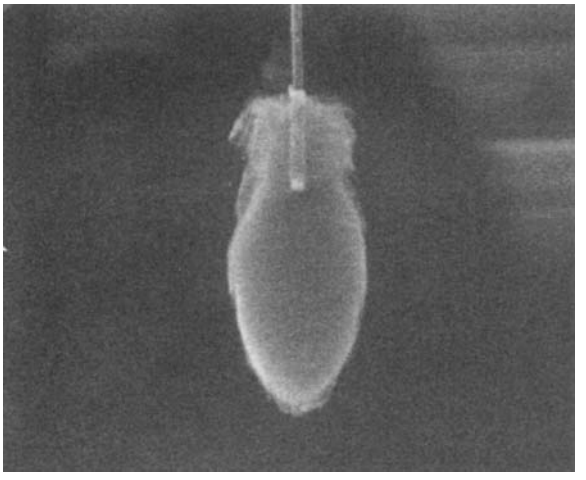

FIGURE 4. Photograph from the side of a high-aspect-ratio ($a = 2.1$) lens during injection. $N/f = 0.18$, $t = 120$ s ($25T$), $\alpha N/f = 0.4$.

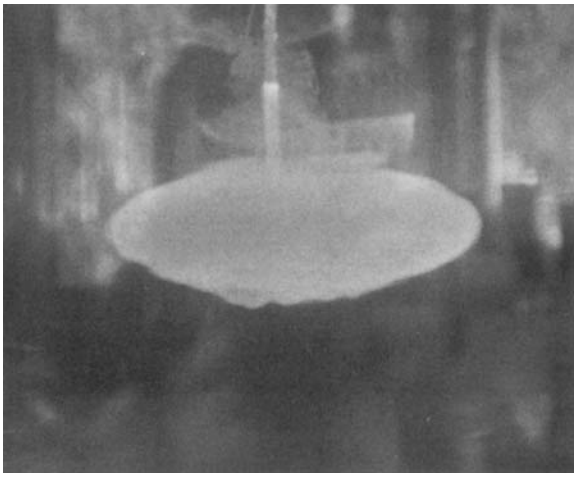

FIGURE 5. Photograph from the side of a low-aspect-ratio ($\alpha = 0.4$) lens during injection. $N/f = 1.3$, $\alpha N/f = 0.5$.

approximately 1 cm. There are several known axisymmetric instabilities: inertial instability and two instabilities of a baroclinic circular vortex, with and without diffusion.

For inertial stability, the magnitude of the total circulation $|2\pi rv + \pi fr^2|$ must increase with radius (cf. Eliassen & Kleinschmidt 1957, section 25). For an anticyclonic lens this requirement is always satisfied unless the core Rossby number is greater than 0.5. A Rossby number greater than 0.5 implies that the lens is spinning in the opposite direction to the tank in the laboratory frame of reference. The lens interior circulation would then be negative, with positive circulation outside and an unstable region in between where the circulation vanishes. Our laboratory source of fluid determined the initial potential vorticity of the injected lens and always produced inertially stable lenses with Rossby numbers less than 0.5.

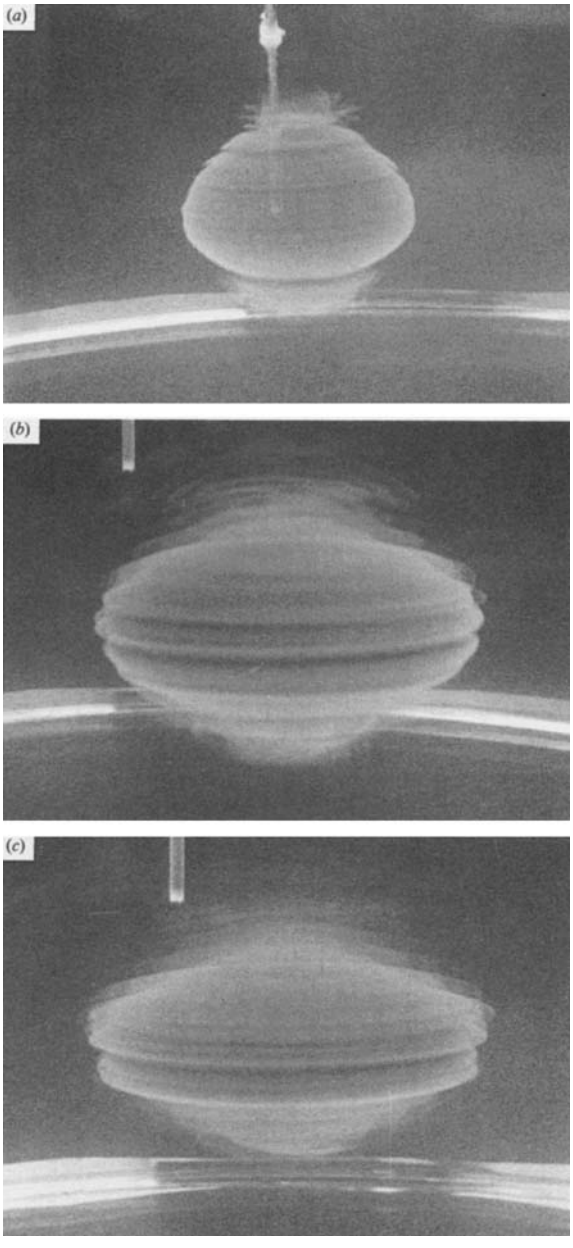

FIGURE 6. Photographs of a lens as seen from the side showing the time evolution of an axisymmetric instability. $N/f = 0.53$. (*a*) During injection: $t = 120$ s ($13T$), $\alpha = 0.7$, $\alpha N/f = 0.4$; (*b*) $t = 250$ s ($26T$ after injection); (*c*) $t = 600$ s ($65T$ after injection).

For a baroclinic circular vortex in polar coordinates the linear stability criterion becomes

$$Ri > \frac{f+2\frac{v}{r}}{f+\frac{v}{r}+\frac{\partial v}{\partial r}}, \tag{3.1}$$

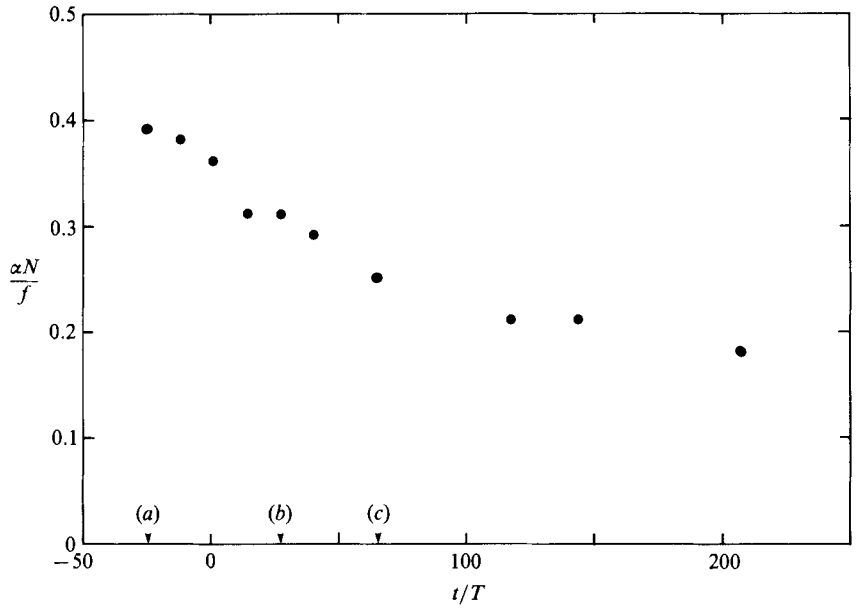

FIGURE 7. $\alpha N/f$ *vs.* t/T for the lens shown in the photographs of figure 6.

where Ri is the Richardson number (cf. Eliassen & Kleinschmidt, 1957 section 26; Ooyama 1966). This criterion reduces to $Ri > 1$ for stability in the solid-body core of Gill's model. This instability has no preferred spatial scale in an infinitely large domain.

The McIntyre (1970) instability is similar, but includes diffusive terms for both salt and momentum. The linear stability criterion then becomes

$$Ri > \frac{f(\sigma+1)^2}{4\sigma\left(f+\frac{\partial v}{\partial r}\right)}, \tag{3.2}$$

where $\sigma = \nu/\kappa$. For salt water $\sigma = 700$ leading to $Ri > 175$ for stability.

For lenses created in the laboratory, for example in figure 6(*b*, *c*), and also in Griffiths & Linden (1981, figure 16*a*), the layering seen above and below the lens, as well as its angle with respect to the vertical is a distinctive signature of the McIntyre instability (Calman 1977). In §5, after describing the velocity and density fields, we estimate the Richardson number and find $Ri \geqslant 6$, also indicative of the McIntyre instability.

4. Velocity fields

As described in §2, the velocity field was measured using particle streak photography, which unless otherwise noted was at the equatorial level. Figure 8 shows speed *vs.* radius for one lens at five successive times, with Gill's model included for comparison. The core is in nearly solid-body rotation. The speed near the edge of the lens decreased from 3 cm s^{-1} to 1 cm s^{-1} over 150 rotation periods.

The scatter in the speed *vs.* radius in figure 8 can be attributed to uncertainty in each measurement as well as the lens deviating from axisymmetry: the standard

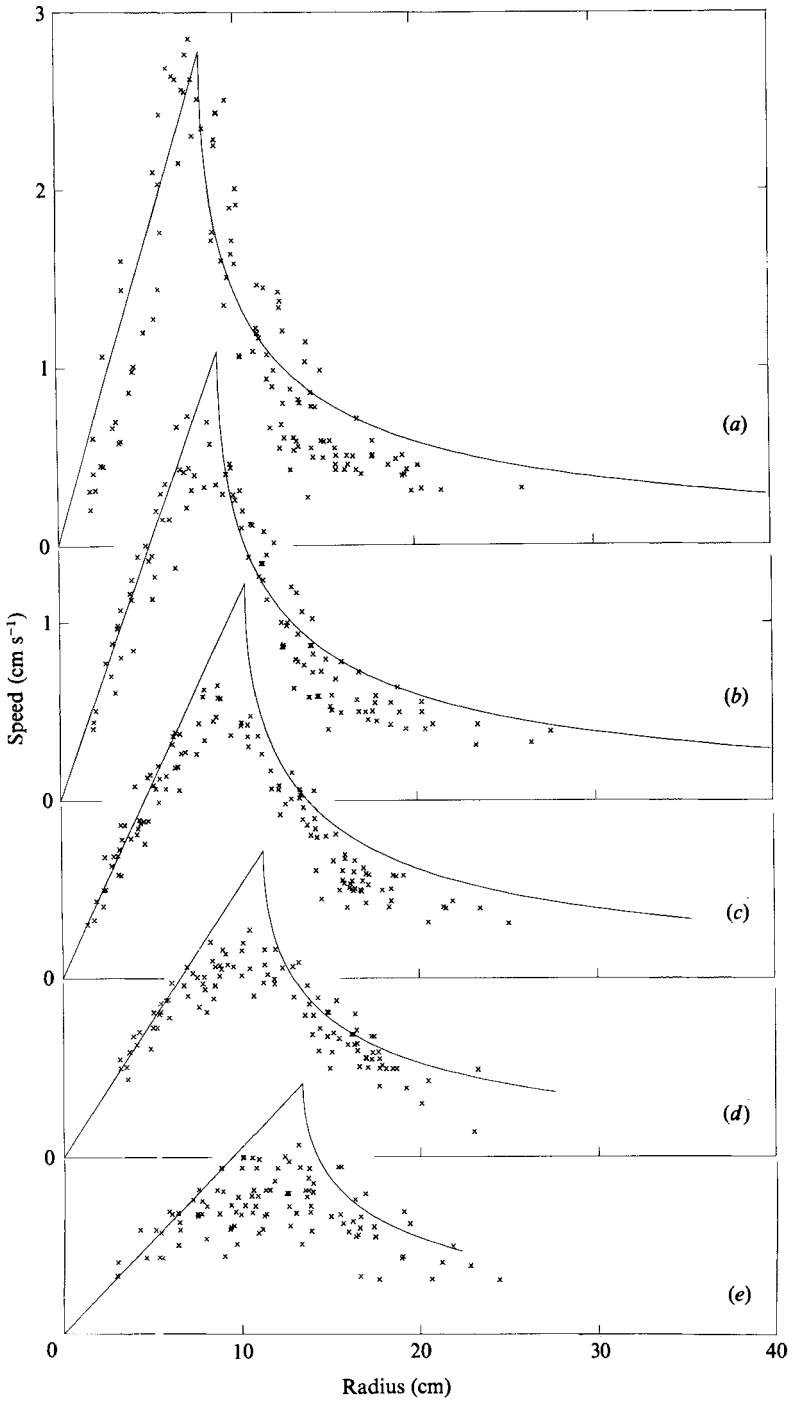

FIGURE 8. Speed *vs.* radius for five different normalized times ($t/T = 0$ is when injection ended). Gill's model is shown as a solid line for comparison: $N/f = 0.80$, $n = 1.00$ s^{-1}, $f = 1.27$ s^{-1}. (*a*) $h_0 = 2.75$ cm ($t/T = 6$), (*b*) $h_0 = 2.5$ cm ($t/T = 21$), (*c*) $h_0 = 2.2$ cm ($t/T = 48$), (*d*) $h_0 = 1.7$ cm ($t/T = 87$), and (*e*) $h_0 = 1.4$ cm ($t/T = 172$).

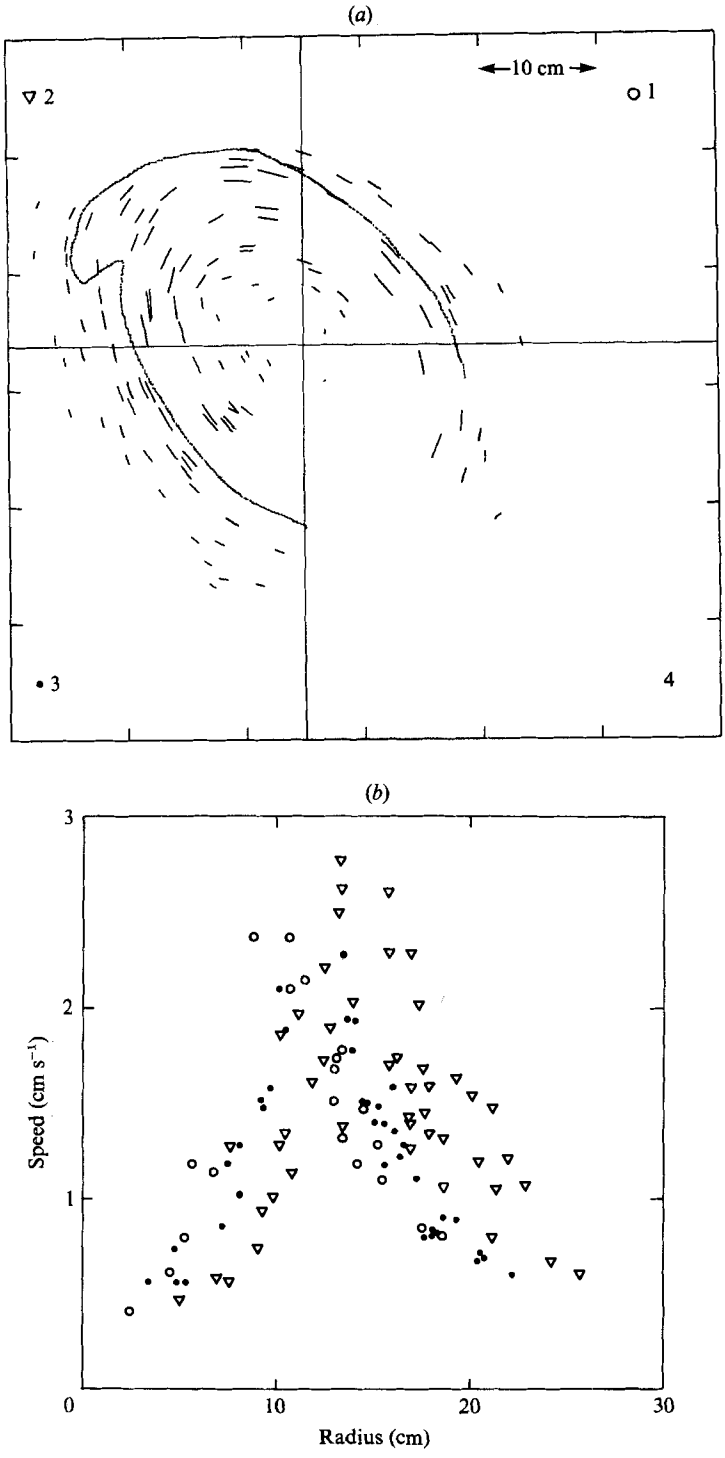

FIGURE 9(*a*). Digitized data for an asymmetric lens showing the corrected streaks and the outline of the dyed fluid. $N/f = 1.19$, $t = 25$ s ($2T$ after injection). (*b*) Speed *vs.* radius for three of the quadrants in (*a*).

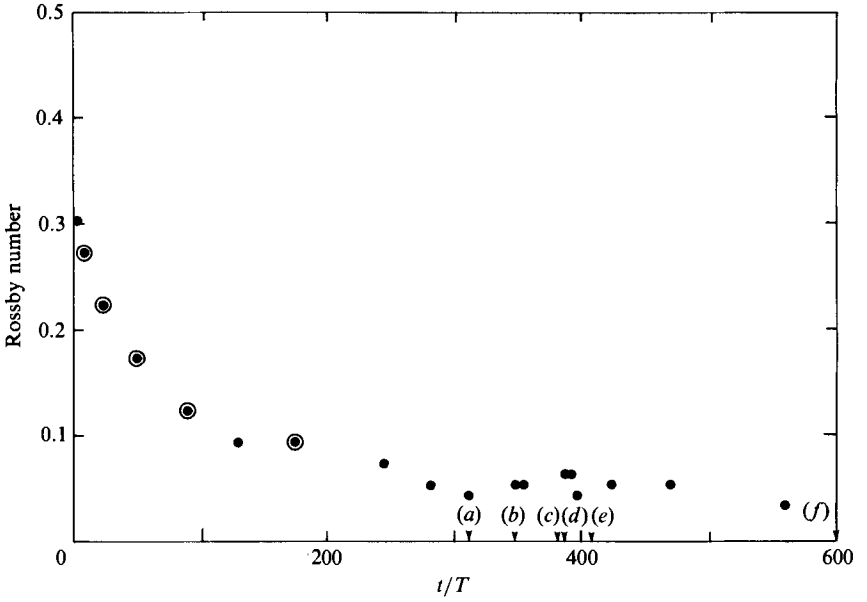

FIGURE 10. *Ro vs. t/T*. Circled points correspond to times also shown in figure 8, arrows correspond to times of photographs in figure 17.

deviation in velocity is 1 mm s^{-1}. Lenses are often not completely axisymmetric; the lens shown in figure 9(*a*) is an extreme example. Figure 9(*b*) shows speed *vs.* radius for three of the four quadrants of this lens. In this extreme case, the velocity *vs.* radius becomes more scattered; particles move faster, at a given radius, in quadrants for which the distance to the edge of the lens is least (see figure 9*a*, *b*). The variability of speed *vs.* radius seen at $t/T = 172$ in figure 8 is due almost entirely to the lens asymmetry.

The angular velocity of the core, computed from the velocity data, was used in the fit to Gill's model at various times in figure 8. In order to calibrate our ability to measure angular velocity, a photograph of the night sky was digitized and processed to yield 7.0×10^{-5} for the angular velocity, within 3% of the actual value. The Rossby number is plotted in figure 10 for this lens, with the times in figure 8 marked by the circled dots. The early decay is rapid; the Rossby number is half its initial value after 70 rotations. At later times the Rossby number remains nearly constant and a different final decay process, associated with shedding, is evident and will be discussed in §6. The motion in the exterior fluid changes very little with time, as can be seen in figure 8.

Figure 11 shows Rossby number *vs.* time for seven different experiments: time has been normalized by the rotation period. The injected fluid has zero potential vorticity, which would lead to an initial Rossby number of 0.5. The measured initial Rossby numbers differ and are all less than 0.5 owing to mixing during the injection. The characteristics of the injection are determined by the flow rate Q and the mechanics of the injector. Although the initial Rossby numbers differed for each experiment, the early decay scales simply by an Ekman timescale $\tau_e = Nh_0/f(2\nu f)^{\frac{1}{2}}$, as seen in figure 12. Helfrich (1987) found a similar, although not identical, scaling to be appropriate. An approximate fit through our data in figure 12 gives a half-life of $40\tau_e$.

All of the data described so far have been at the equatorial level of the lenses.

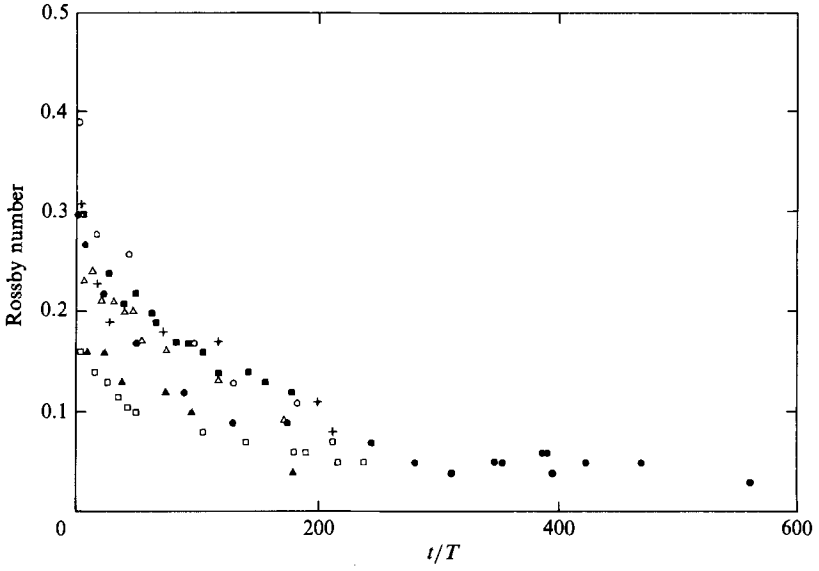

FIGURE 11. *Ro vs.* t/T for seven different lenses. The experimental parameters are given in table 1.

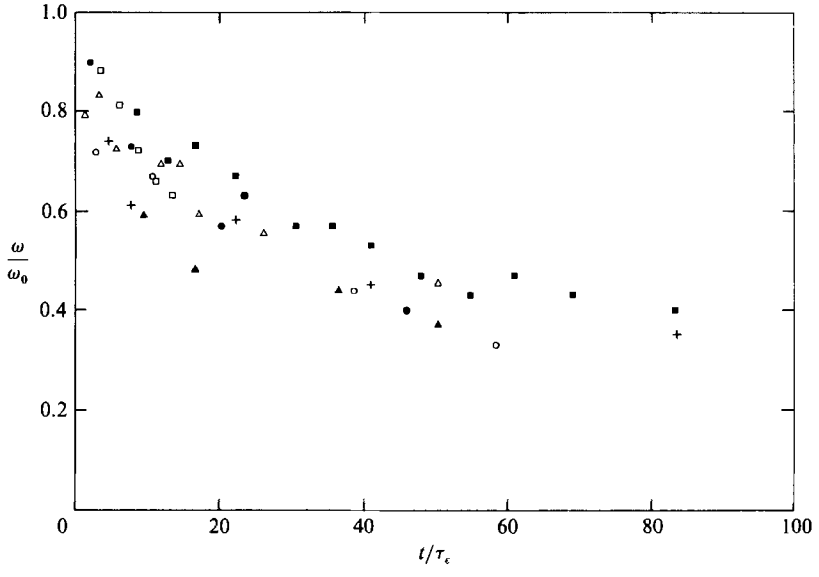

FIGURE 12. ω/ω_0 *vs.* $\tau_\epsilon = Nh_0/f(2\nu f)^{\frac{1}{2}}$. The symbols are given in table 1.

Figures 13 and 14 show non-dimensional speed as a function of non-dimensional radius at four different levels for two different experiments; Gill's model is again shown for comparison. The radius of the fluid moving as a solid body was similar at all levels, extending above and below the lens of dyed fluid, as shown in the inset diagram. Within a homogeneous lens the velocity is independent of height, as suggested by the Taylor–Proudman theorem.

Both Gill's model and the data suggest that in the stratified regions above and below the homogeneous core the velocity distribution at any level has a central

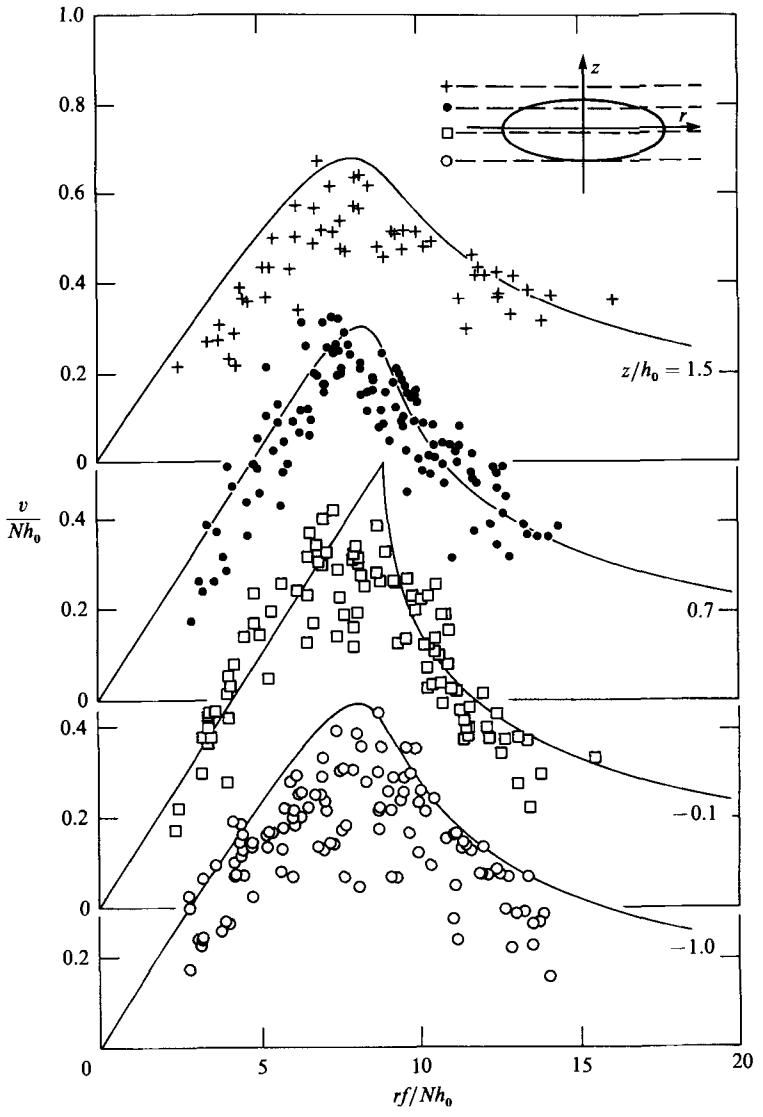

FIGURE 13. Speed *vs.* radius at four different levels, as shown in the inset. Gill's model is shown as a solid line for the various levels, where the Rossby number at the central level determines the fit. $N/f = 1.19$, $N = 1.19\ \text{s}^{-1}$, $f = 1.00\ \text{s}^{-1}$, $h_0 = 1.95$ cm, $t/T = 29$–34.

portion of constant vorticity which is less than that in the homogeneous core. Figure 15 shows Rossby numbers *vs.* time for the lens in figure 13 at all the levels for which we have data.

In figures 8, 13, and 14, Gill's model has been shown with the data. Among all models proposed it is the only one to account for motion in the exterior fluid due to the injection. The model neglects friction and the equations are in Cartesian coordinates, implying a flow parallel to the y-axis and independent of y. These equations are only strictly valid in the cylindrical geometry if the Rossby number $Ro \ll 1$. Nonetheless the model appears suitable even at Rossby numbers as large as 0.3 (figure 8).

Gill's equations are non-dimensionalized by scaling z with the lens thickness h_0,

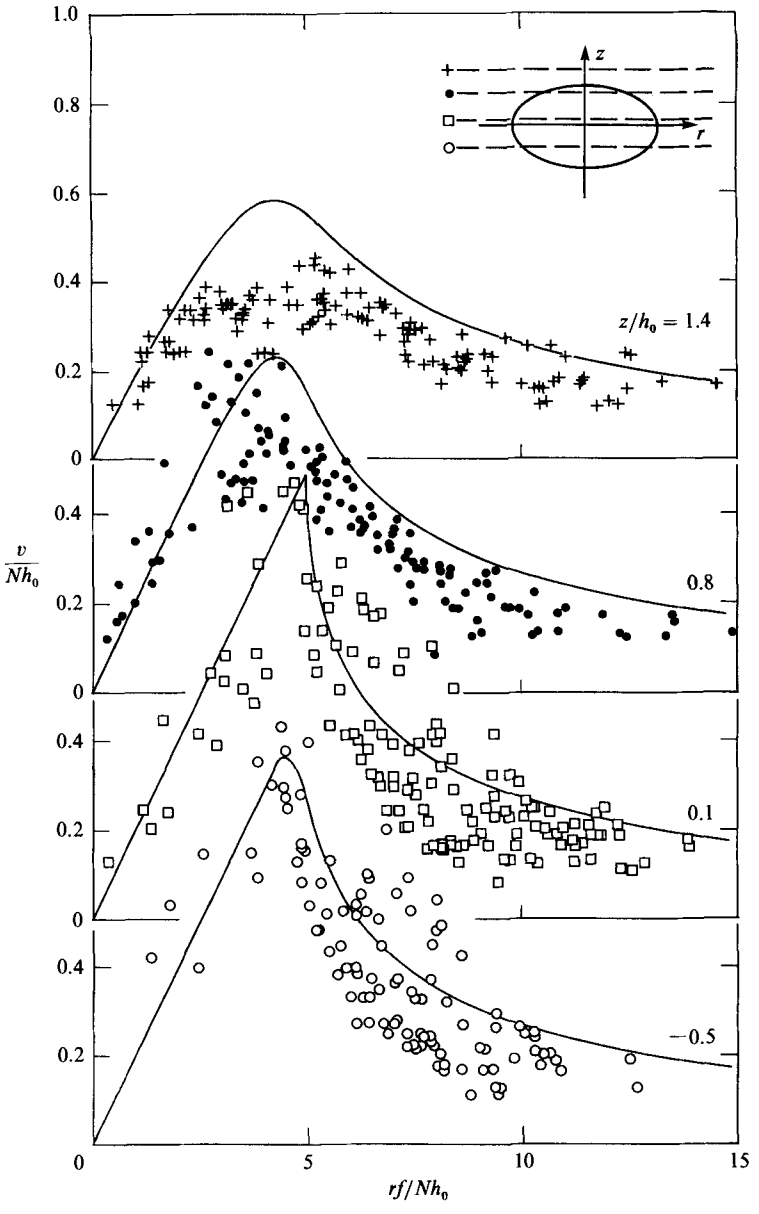

FIGURE 14. Speed *vs.* radius at four different levels, as shown in the inset. Gill's model is shown as a solid line for the various levels, where the Rossby number at the central level determines the fit. $N/f = 0.36$, $N = 0.65\ \mathrm{s}^{-1}$, $f = 1.80\ \mathrm{s}^{-1}$, $h_0 = 4.0$ cm, $t/T = 26$–29.

x with Nh_0/f (implying an aspect ratio proportional to f/N), and v with Nh_0. The resulting equations have only one parameter, a, the non-dimensional radius of the lens, which is equal to Ro^{-1}. Among the three model scaling constants N, f, and h_0, both N and f were well determined in the experiments. We found that the model best fitted the velocity data when a lens thickness h_0 of approximately 90% of the measured thickness of the dye was used. This difference is due to the diffusion of dyed fluid into the background stratification during the initial injection, the extent of which was not studied in detail.

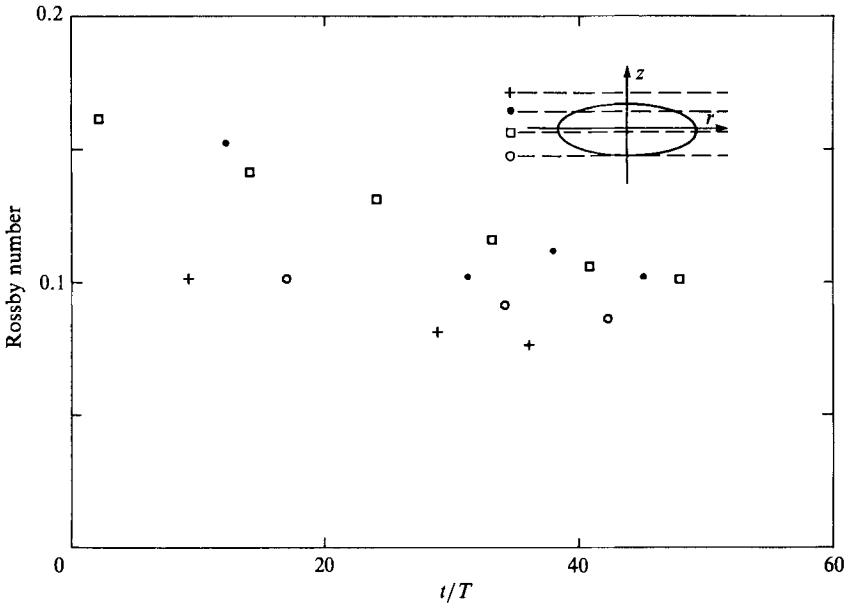

FIGURE 15. *Ro vs. t/T* at four different levels (see insert) derived from speeds as shown in figure 13.

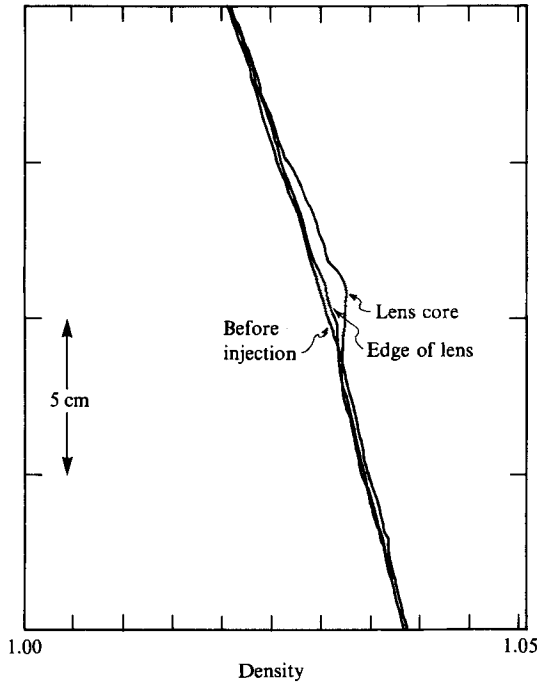

FIGURE 16. Density as derived from conductivity data before a lens is injected, through the lens core, and at the lens edge.

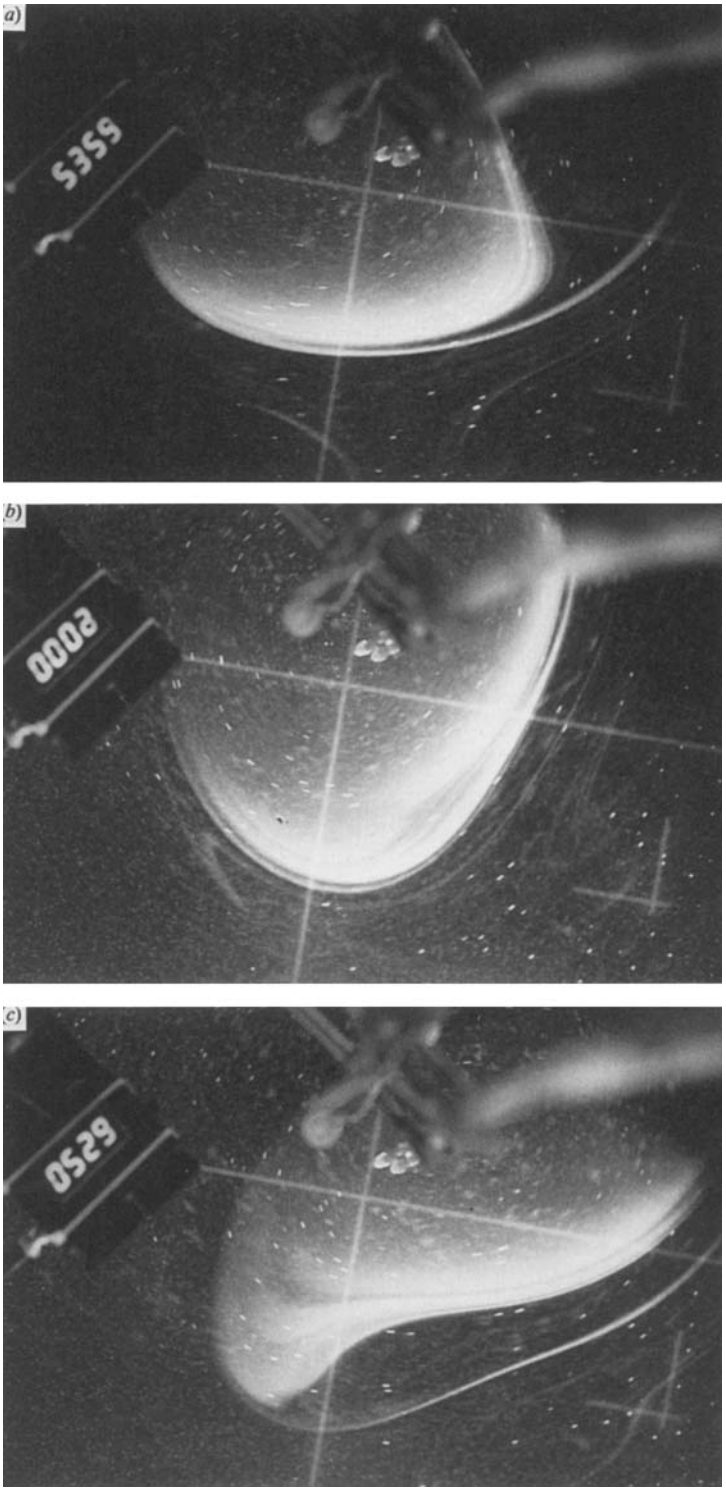

FIGURE 17 (*a–c*). For caption see facing page.

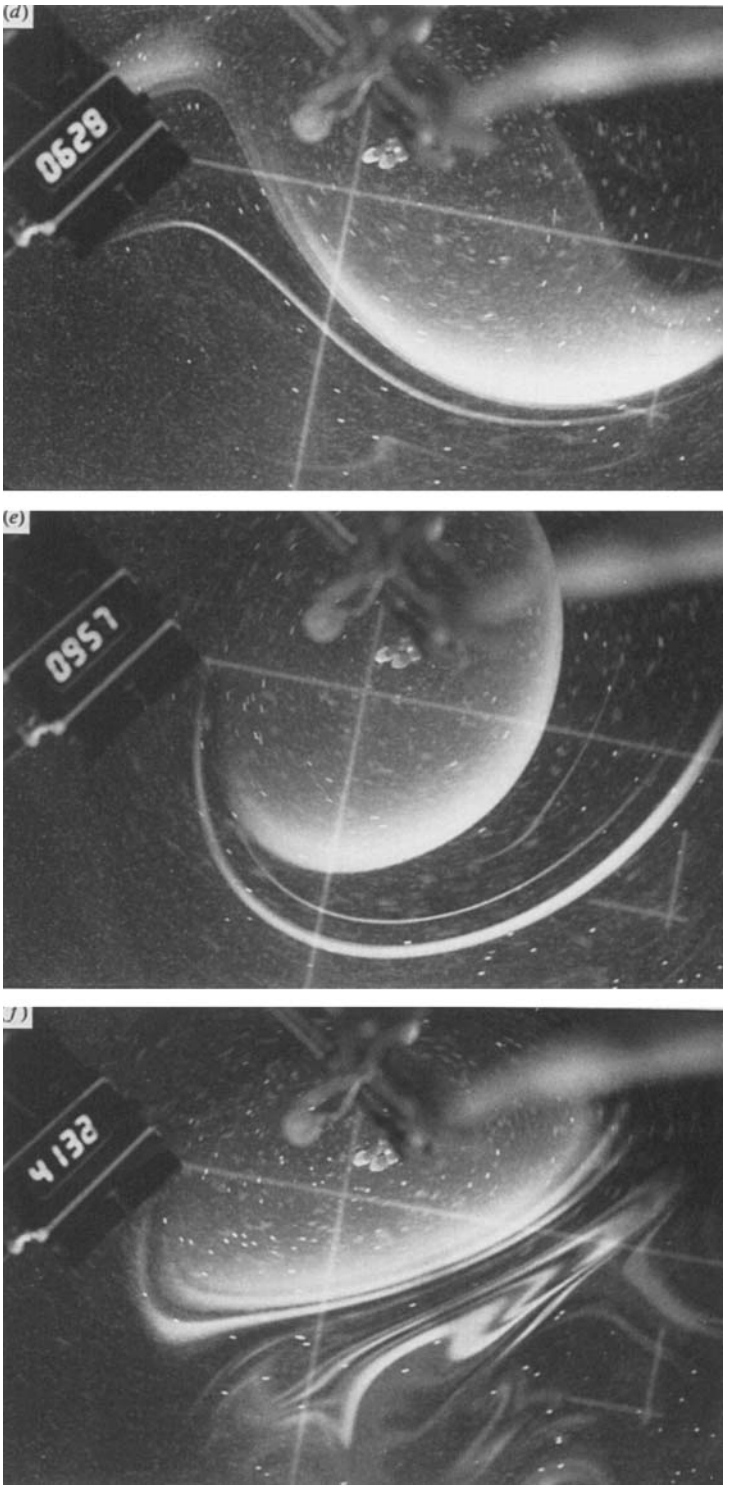

FIGURE 17. Photographs showing lens evolution for times greater than 300 table rotation periods: $N/f = 0.80$ (*a*) $t/T = 309$, (*b*) 345; (*c*) 379; (*d*) 384; (*e*) 406; (*f*) 596.

5. Conductivity measurements and Richardson number

A few conductivity measurements were made before and after a lens was formed. Unfortunately, the conductivity probe disturbed the lens and caused premature shedding; hence these measurements were only taken occasionally. A typical example, figure 16, shows that the initial stratification was linear to within experimental error and the interior of the lens was homogeneous. No temperature corrections were made although the lens was apparently slightly warmer than the surrounding fluid and its higher conductivity, uncorrected for temperature, appears as a higher salinity. The probe's spatial resolution of 4 mm was too coarse to resolve layering above and below the lens caused by the McIntyre instability.

In spite of these limitations, the conductivity measurements show that density is distributed over a vertical scale significantly larger than the limiting 4 mm resolution, allowing us to estimate the Richardson number. The density gradient exterior to the homogeneous core remains close to that of the background stratification. The largest shear in figure 14 is 0.3 s^{-1} between the uppermost levels, corresponding to $Ri \approx 6$ at a radius of $rf/Nh_0 = 4$. The shear decreases as the lens decays; the smallest Richardson numbers occur immediately after lens formation.

This value indicates stability with respect to the inviscid theory of Ooyama (1966) and instability with respect to the McIntyre (1970) double-diffusive instability for mass and momentum. The minimum values of the Richardson numbers required for stability are $Ri = 1$ (equation (3.1)) and $Ri = 175$, (3.2), respectively. Also, the distinctive layering seen above and below the lenses, as well as the slope of the layered structure, was identical to that seen by Calman (1977) in his studies of the McIntyre instability.

6. Final decay

When the injection is laminar, an axisymmetric lens is formed. More-turbulent injections produced lenses that were initially not axisymmetric; only after several minutes did these lenses approach symmetry. Part of the process by which this happens can be seen in figures 3 and 9(*a*) where some dyed fluid was shed from the lens; in figure 9(*a*) the lens has a large cusp while in figure 3 the shed dye is a fossil tracer. Once near circular, a lens is stable to asymmetric instabilities during the time that the core Rossby number decays rapidly. The lens for which the Rossby number is shown in figure 10 was nearly axisymmetric until $t/T \approx 150$.

Shedding in the equatorial plane begins with the lens becoming elliptically deformed, often with one end narrower than the other. The narrow end (or ends) then become cusped and appear sheared by the flow at the edge of the lens. Undyed fluid is entrained between the shed fluid and the remaining lens core. The core then becomes circular again, only to shed once more at a later time. The shedding cycle typically occurs every 30–50 rotation periods.

This process is illustrated in figure 17 (*a–f*), a sequence of photographs taken after shedding started. Figure 17(*a*) shows the lens at $t/T = 309$ with a cusp in the lower-right quadrant of the sort that typically leads to shedding. In addition, dyed fluid that was previously shed is visible in the exterior fluid. In figure 17 (*b*) ($t/T = 345$) this previously shed fluid was wrapped around the lens. Figure 17 (*c*) ($t/T = 379$) shows a large perturbation on the lens where mixed fluid at the edge was being shed. This process continued in figure 17 (*d*) ($t/T = 384$), which shows two cusps on opposite sides shedding simultaneously. In figure 17 (*e*) ($t/T = 406$) the core of the lens is nearly

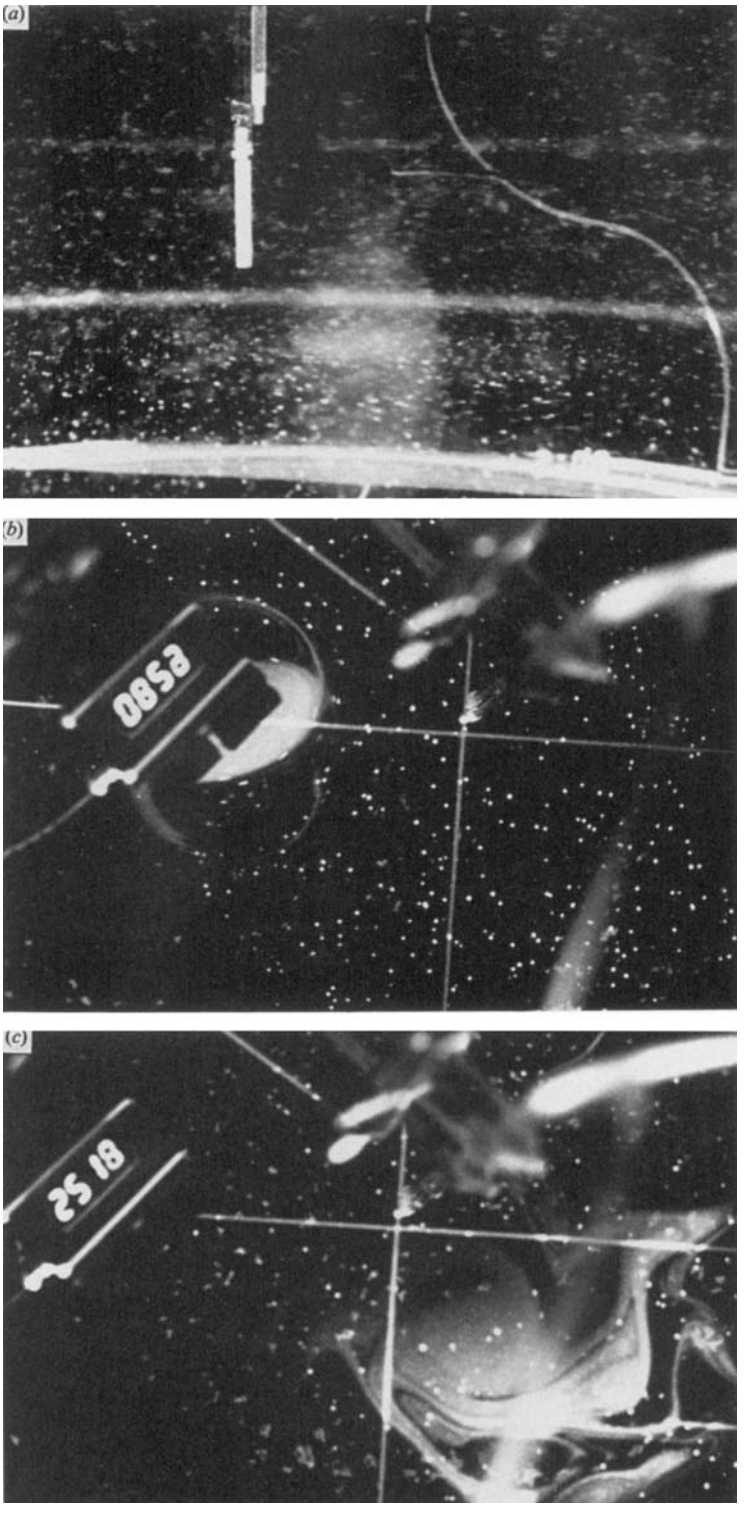

FIGURE 18. (*a*) Side view of a lens that was in close proximity to the bottom of the tank. $N/f = 0.21$, $t = 320$ s, $t/T = 45$. (*b*) Top view of the lens in (*a*). $t = 290$ s, $t/T = 41$. (*c*) Top view of the same lens at a later time. $t = 1260$ s, $t/T = 180$.

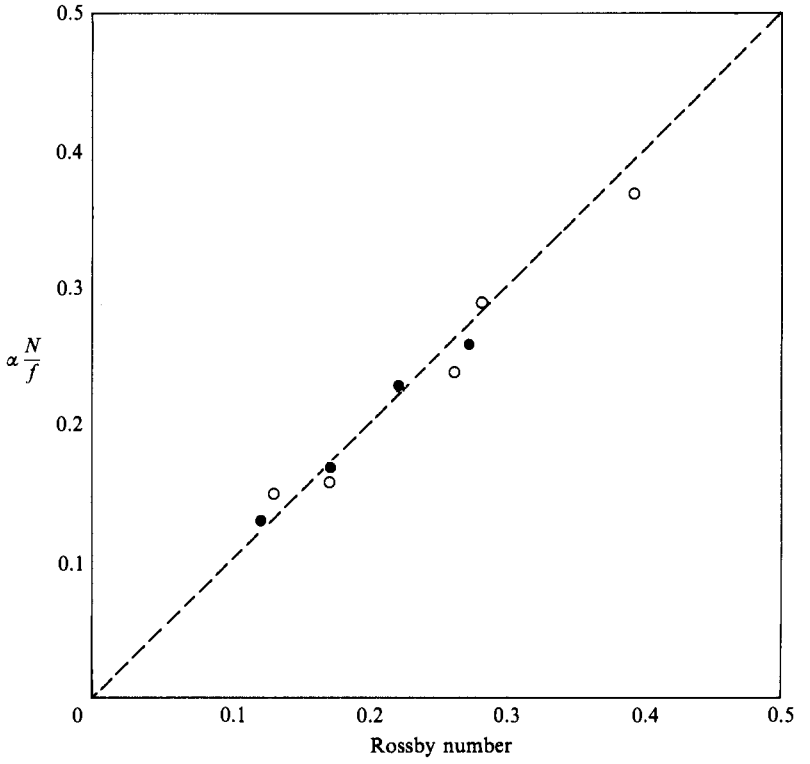

FIGURE 19. $\alpha N/f$ *vs.* *Ro*. The symbols are as in table 1. The dashed line through the data is $\alpha N/f = Ro$ as predicted by Gill's model.

circular again and the previously shed fluid is no longer near the lens core. Figure 17 (*f*) ($t/T = 596$) shows the lens and the background fluid after several more such events have taken place.

Figure 10 shows Rossby number *vs.* time for this particular lens with the times of the photographs used in figure 17 marked. The initial decay was exponential until the Rossby number decreased to approximately 0.06, after which the Rossby number was nearly constant for an extended period. During this extended period slower fluid was repeatedly shed from the edge of the lens. The cause of this shedding remains unclear, but there is a possible explanation in the theoretical literature for lenses of density ρ_1 overlaying fluid of density ρ_2. A full discussion will be deferred to the conclusion.

Our stability criterion differs from that observed by Griffiths & Linden (1981). The difference is due to the fact that our lenses were formed in a stratified background. In contrast, Griffiths and Linden performed their experiments with two fluids of different densities. Owing to the Taylor–Proudman theorem, the motion exterior to their eddies extended to the bottom (cf. their figure 12 and discussion of $\delta = h/H$, the fraction of the fluid depth occupied by the lens). The stratified background fluid of our experiments isolated our lenses from both the top and the bottom of the tank.

We do not fully understand the results for instability at $N/f < 0.4$ reported by Helfrich (1987). However, one of our experiments with a lens close to the bottom, (figure 18*a–c*) yielded instabilities with signatures (figure 18*b*) similar to those reported by Helfrich. At longer times (figure 18*c*) very complex structures evolved.

It is not N/f that appears to be important: lenses with the same value ($N/f = 0.2$) and lenses at mid-depth in the tank, away from the bottom, did not become unstable. At these low values of N/f lenses are tall and thin (figures 4 and 18*a*). One must be certain that the exterior flow field, which has the same aspect ratio as the lens, does not extend to the top or bottom of the container.

7. Conclusion

Careful injection of a homogeneous fluid, into a linearly stratified and rotating background fluid, produced anticyclonic lenses which were studied for up to 600 table rotation periods. Velocity measurements (cf. figure 8) using streak photography have shown that the interior core rotates as a solid body with a decreasing, nearly axisymmetric exterior velocity field. The edge of the dyed injected fluid was always found outside the radius of maximum velocity and well outside the radius of the solid-body core. The velocity measurements are well predicted by Gill's (1981) model (cf. figures 8, 13, 14). His model also predicts that the aspect ratio is related to the Rossby number by

$$Ro = \alpha \frac{N}{f}. \tag{7.1}$$

This is shown in figure 19 which includes our data from two experiments.

Lens decay occurred in two stages: symmetric rapid spin-down during the first 100 table rotation periods, followed by an asymmetric shedding instability.

The symmetric rapid spin-down, as illustrated in figures 10–12, has an associated half-life of $\approx 40\tau_\epsilon$. The spin-down is from the initial lens Rossby number, which ranged from 0.17 to 0.4 depending on entrainment at the injector, to a final Rossby number, $Ro \approx 0.06$. For a lens in which we have velocity data at four levels, we estimate the minimum value of the Richardson number to be $Ri \approx 6$. This value and the distinctive layering seen confirm the instability to be of the type first discussed by McIntyre (1970).

Once the core Rossby number reaches the value $Ro \approx 0.06$, it remains nearly constant for up to 500 additional table rotation periods (figure 11). Core size decreases through a repeated process of shedding slower fluid from the lens periphery (figures 17*a–f*). The following theories provide some insight into the shedding process. Killworth (1983) showed that a circular lens in isolation is stable to small perturbations. Cushman-Roisin (1986) showed that elliptical lenses of more than a critical ellipticity are unstable to a mode-three perturbation. Our lenses are in a stratified fluid, possibly leading to a different critical eccentricity, but the qualitative result is probably the same. Melander, McWilliams & Zabusky (1987) report that their numerical-model lenses axisymmetrize through a process of shedding filaments. These studies show that a circular lens is stable and that an elliptical lens will become unstable in such a way as to axisymmetrize the lens. The question then remains as to how a lens becomes elliptical. Ruddick (1987) shows that strain in the surrounding fluid will cause a lens to become eccentric. Figure 2 shows that the flow before a lens is injected has a very small, but non-zero strain. As the lens spins down, the non-zero background strain becomes relatively stronger and may be responsible for the ellipticity.

We are particularly grateful to Professor Fred Browand who gave us photographs of his preliminary experiments and then made available to Ms Hedstrom experimental facilities at the University of Southern California for initial feasibility

studies. Space for setting up the experimental facility was made available to us by the Institute of Geophysics and Planetary Physics (SIO) and we appreciate their hospitality. Dr Don Altman gave helpful advice, especially on streak photographic technique. This research was founded by the National Science Foundation Physical Oceanography Program; start up funding was provided by the Scripps Institution of Oceanography.

REFERENCES

ARMI, L. & ZENK, W. 1984 Large lenses of highly saline Mediterranean water. *J. Phys. Oceanogr.* **14**, 1560–1576.

CALMAN, J. 1977 Experiments on high Richardson number instability of a rotating stratified shear flow. *Dyn. Atmos. Oceans* **1**, 277–297.

CUSHMAN-ROISIN, B. 1986 Linear stability of large, elliptical warm-core rings. *J. Phys. Oceanogr.* **16**, 1158–1164.

DUGAN, J. P., MIED, R. P., MIGNEREY, P. C. & SCHUETZ, A. F. 1982 Compact intrathermocline eddies in the Sargasso Sea. *J. Geophys. Res.* **87**, 385–393.

ELIASSEN, A. & KLEINSCHMIDT, E. 1957 Dynamic meteorology. In *Handbuch der Physik, vol.* 48, *pp.* 1–154.

GILL, A. E. 1981 Homogeneous intrusions in a rotating stratified fluid. *J. Fluid Mech.* **103**, 275–295.

GRIFFITHS, R. W. & LINDEN, P. F. 1981 The stability of vortices in a rotating, stratified fluid. *J. Fluid Mech.* **105**, 283–316.

HEDSTROM, K. 1985 Salt lenses in the laboratory. *EOS* **66**, 1311.

HEDSTROM, K. 1986 Laboratory salt lenses. *EOS* **67**, 1061.

HELFRICH, K. R. 1987 Experiments on baroclinic eddy evolution and stability in rotating continuously stratified systems. *Preprints, Third Intl Symp. on Stratified Flows*, vol. 2, B4, pp. 1–10. IAHR, AGU, ASCE.

KILLWORTH, P. D. 1983 On the motion of isolated lenses on a beta-plane. *J. Phys. Oceanogr.* **13**, 368–376.

MANLEY, T. O. & HUNKINS, K. 1985 Mesoscale eddies of the arctic ocean. *J. Geophys. Res.* **90**, 4911–4930.

MCINTYRE, M. E. 1970 Diffusive destabilization of the baroclinic circular vortex. *Geophys. Fluid Dyn.* **1**, 19–57.

MCWILLIAMS, J. C. 1985 Sub-mesoscale, coherent vortices in the ocean. *Rev. Geophys.* **23**, 165–182.

MELANDER, M. V., MCWILLIAMS, J. C. & ZABUSKY, N. J. 1987 Axisymmetrization and vorticity gradient intensification of an isolated two-dimensional vortex through filamentation. *J. Fluid Mech.* **178**, 137–160.

OOYAMA, K. 1966 On the stability of the baroclinic circular vortex: a sufficient criterion for instability. *J. Atmos. Sci.* **23**, 43–53.

RUDDICK, B. R. 1987 Anticyclonic lenses in large-scale strain and shear. *J. Phys. Oceanogr.* **17**, 741–749.

SAUNDERS, P. M. 1973 The instability of a baroclinic vortex. *J. Phys. Oceanogr.* 3, 61–65.